MCEN90032
Sensor Systems

Workshop #2 - Indoor GPS System

Xing Yang Goh
1001969
Apr 28, 2021

1 Introduction

The objective of this workshop is to design an indoor GPS, which purpose is to use the functionality of a smartphone's IMU sensor to estimate the path without using the Global Navigation Satellite System (GNSS). This report will focus on the development of two facets of the design:

1. A Kalman filter using the Magnetometer and Gyroscope to acquire the heading direction.
2. A distance estimator using the designed pedometer using an Accelerometer.

This Indoor GPS extends the pedometer designed in workshop one and will not cover the pedometer implementation. This report will focus on the heading direction algorithm and a distance estimator algorithm using the pedometer. The sensors used and the axes of measurements are detailed below:

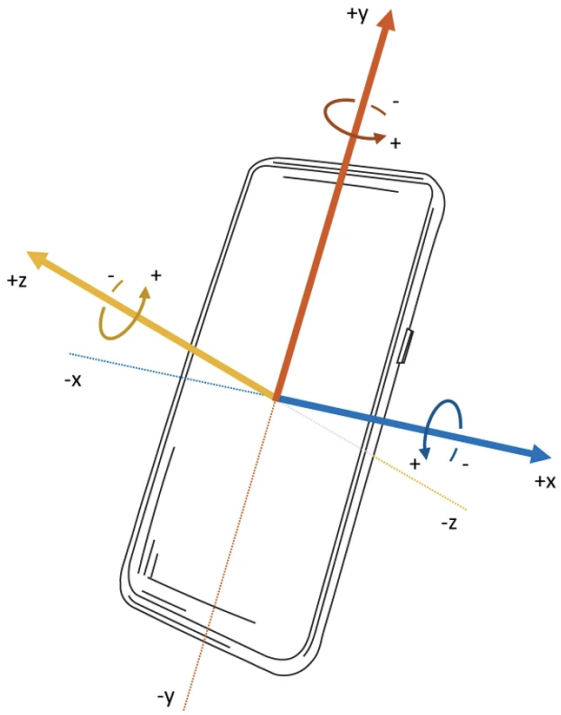

Figure 1: Smartphone IMU measurement axes

1. **Accelerometer:** Measures the 3-axis rate change of velocity in $(\frac{m}{s^2})$
2. **Magnetometer**: Measures the 3-axis strength of Earth's magnetic field (μT)
3. **Gyroscope**: Measures the angular velocity around the 3 axes of the smartphone $(\frac{rad}{s})$
4. **GPS**: Measures the geolocation of the smartphone with latitude, longitude and altitude information (°)

2 Methods

2.1 Data Acquisition

The sampling frequency chosen adheres to the minimal Nyquist frequency to ensure that there is no distortion from aliasing effects. The model for heading direction using the gyroscope requires an

integration of the angular velocity or a forward Euler method using the sampling period as each time step. Therefore, a sampling frequency of 50Hz is chosen to ensure an accurate discretisation of the analog angular velocity without being computationally expensive. This acquired data links to the MATLAB cloud drive for further analysis.

In order to test the efficacy of the indoor GPS, this data will be recorded outdoors for comparisons with latitude and longitude data using the built-in GPS in the smartphone. The path taken will be around the Old Engineering building.

2.2 Sensor Calibration

We must calibrate the magnetometer measurements to account for the soft and hard iron effects. The soft-iron effect causes distortion effects that perturb the measurements from an ideal sphere to an ellipsoid created by nearby metals such as iron. The hard-iron effect generates a constant bias in the sensor output from nearby objects that generate a magnetic field, such as magnetised iron (Ozyagcilar, 2012). The calibration theory will not be detailed in this report, and these calibrations will be performed through the MATLAB function magical.

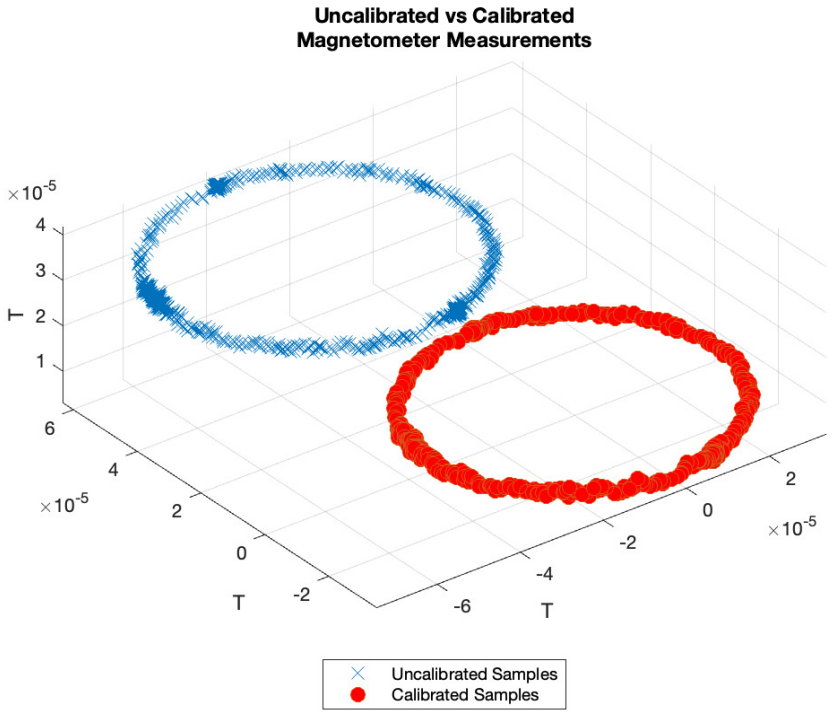

Figure 2: Magnetometer calibration

Figure 14 is an example of the calibrated magnetometer readings during data acquisition, note that the samples form a circle instead of a sphere because the phone is held with a constant pitch angle during the tests so no tilt compensation from the orientation of the phone is required.

For the gyroscope, the deflection from the vertical axis from the normal to the Earth ellipsoid causes the measured angular velocity to be lower than the actual value (Kaniewski & Kazubek, 2009). To account for this, a constant gain is calculated by numerically finding the gain that minimises the mean square error (MSE) of the heading angle produced by the gyro against the heading angle from the orientometer from a walk around the Old Engineering building. This leads to a gain of 1.05, which results to a MSE of 7.574. Figure 3 shows the gyroscope heading direction using a gain of 1.05.

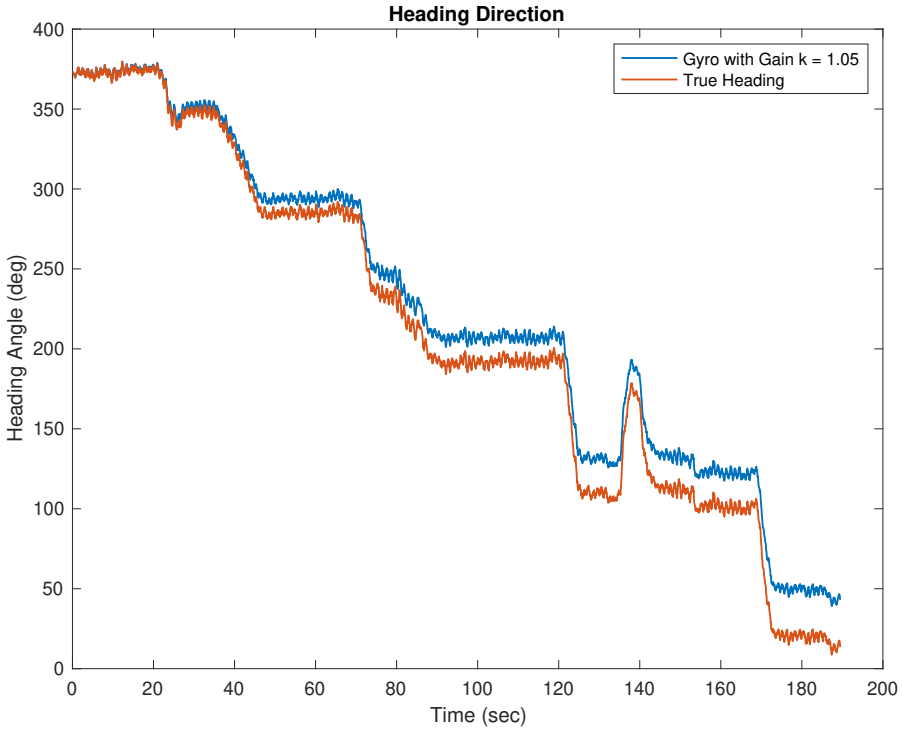

Figure 3: Gyroscope Gain Calibration

3 Distance Estimator

To test a distance estimator, a 32m back and fourth walking experiment is conducted to calculate the cumulative distance using the distance estimator. The first distance estimator implemented is a simple cumulative double integration of the acceleration magnitude in the x-y plane. This will yield the distance travelled at each time step.

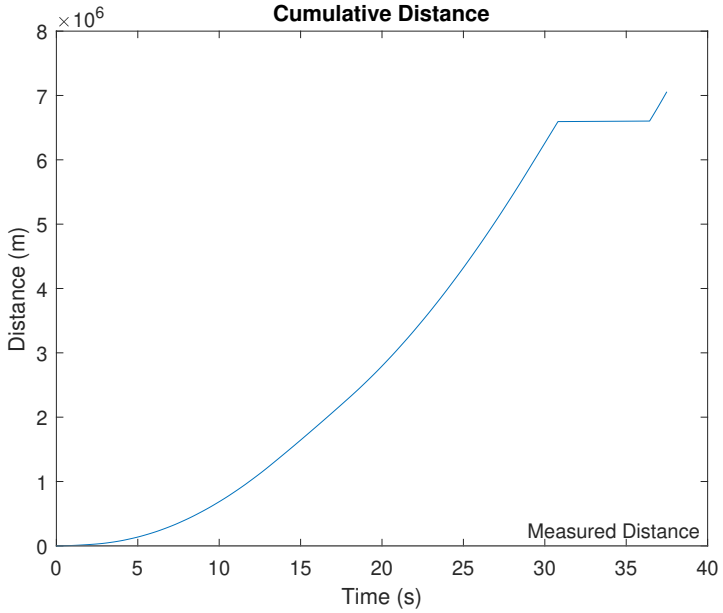

Figure 4: Magnetometer calibration

The integration technique severely overestimates the distance travelled, with a cumulative distance at approximately 7×10^6. This is due to a problem introduced when integrating a signal with Gaussian white noise, which introduces drift leading to an accumulation of errors over time. Since the

signal is integrated twice to get a distance estimate, this drift error is severe and leads to a bad estimate of the distance travelled.

To improve on this distance estimation, an extension of the pedometer is used, aiming to eliminate this drifting effect. After filtering the signal and identifying the steps taken, the minimum and maximum Z-axis acceleration during each step is identified to calculate the step length (Weinberg, 2002).

$$\text{Step Length } = \sqrt[4]{A_{z,\max} - A_{z,\min}} \times K \tag{1}$$

The K in this equation is an empirically found constant depending on the units measured (m) and height of the user. Through testing this value of K is approximated to be 0.33.

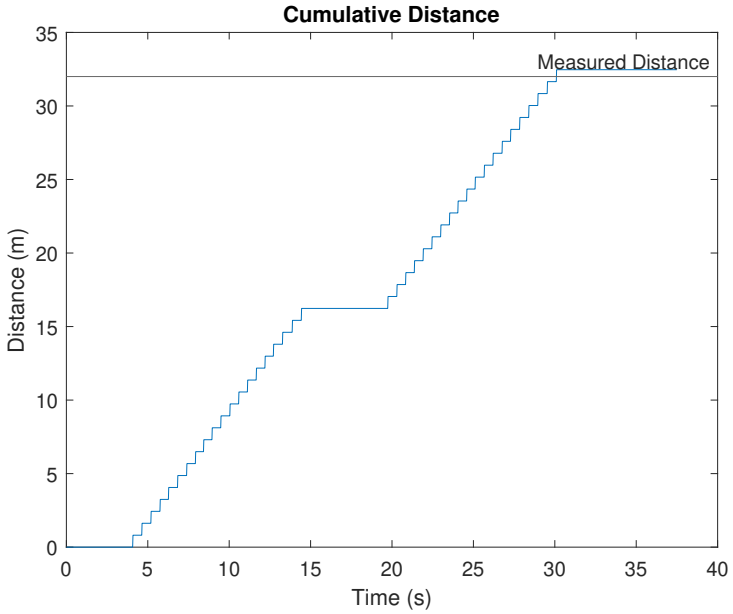

Figure 5: Magnetometer calibration

This adaptive fixed step length algorithm based on the bounce of the user produces a very accurate distance estimate. This algorithm will be the distance estimator of choice for the Indoor GPS.

4 Heading Direction

The chosen continuous-time state space model for the dynamical model of the heading direction is determined as:

$$\dot{\theta} = \omega + v \tag{2}$$

Following this, the observability is described as:

$$y = \omega + w \tag{3}$$

This continuous time state-space dynamics means that the system is fully observable since the matrix T_o of the system is full rank, with x_1 captured with the magnetometer and x_2 captured with the gyroscope. However, the system is not controllable since there is no actuators in the system. This does not inhibit the use of a Kalman filter because it is an optimal observer, and the Kalman gain of an observable system will not diverge to ∞.

$$\theta_{k+1} = \theta_k + \dot{\theta}_k T_s$$

The discretisation method chosen is the backward difference Euler method.

This discretisation method is used since the sampling rate of 50Hz is sufficiently high to get an accurate numerical integration estimation.

4.1 Kalman Filter Design

Before using the Kalman filter, the assumptions of the system must be verified.

1. The random initial condition x_0 is Gaussian with zero mean.
2. Both random processes v_k and w_k are Gaussian white.
3. Two random processes v_k and w_k are independent of each other.
4. Random variable x_0 is independent of two random processes v_k and w_k.

Since the heading angle for the model is initialised to the magnetometer reading, the error of the initial condition will be the error from the magnetometer, which can be assumed as a Gaussian white noise with zero mean since the phone is held at a constant pitch of zero, with the measurement error w_k being a Gaussian white noise as seen in figure 6. The modelling uncertainty error v_k will be a Gaussian white error due to the innate discretised linear dynamics. Since the measurement and model data is acquired using two different sensors, the random processes v_k and w_k are independent of each other. Lastly, the random variable x_0 can be arbitrarily set depending on the desired heading direction, which is not dependent on the measurement or modelling error w_k and v_k.

In order to use this in the Kalman Filter Recursive algorithm, the state vector is predicted from the state dynamics (Rhudy, Salguero, & Holappa, 2017).

$$\hat{\mathbf{x}}_{k|k-1} = \mathbf{F}_{k-1}\hat{\mathbf{x}}_{k-1} + \mathbf{G}_{k-1}\mathbf{u}_{k-1} \tag{4}$$

F and G are the matrices describing the system dynamics, which will be $F = 1$ and $G = T_s$. After finding the predicted state vector $\hat{\mathbf{x}}_{k|k-1}$ is determined using the previous state estimate $\hat{\mathbf{x}}_{k-1}$ and input vector $\mathbf{u}$. The initial state x_0 is initialised using the magnetometer using the equation $\psi_c = 2\pi - \text{atan}\,(H_y/H_x)$, which represents the azimuth angle from the magnetic north (Kaniewski & Kazubek, 2009). Following this, the prediction of the state error covariance matrix is predicted.

$$\mathbf{P}_{k|k-1} = \mathbf{F}_{k-1}\mathbf{P}_{k-1}\mathbf{F}_{k-1}^{T} + \mathbf{Q}_{k-1} \tag{5}$$

Q represents the process noise covariance matrix, which is empirically tuned to be $Q = 0.001$. This parameter represents the state Gaussian noise and uncertainties of the model, which directly affects the amount of smoothing in the Kalman heading estimate. The predicted state error covariance matrix $\mathbf{P}_{k|k-1}$ is calculated using the previous estimated state covariance matrix in a recursive fashion. This means that an initial $\mathbf{P_0}$ must be initialised. This $\mathbf{P_0}$ is an important tuning parameter since a large $\mathbf{P_0}$ value means that the Kalman filter trusts the measurements and gives a low weighting to the state model, with a $\mathbf{P_0}$ of zero completely ignoring the measurements.

$$\mathbf{P}_0 = \left[\frac{1}{N}\sum_{k=1}^{N} F_{k-1}^{\mathrm{T}} H_k^{\mathrm{T}} R^{-1} H_k F_{k-1}\right]^{-1} \tag{6}$$

The initialisation of $\mathbf{P_0}$ is acquired using the Inverse of Information Matrix (IIM), which aims to optimise the choice of $\mathbf{P_0}$ using the covariance of the Gaussian noise for the measurements $\mathbf{R}$, which evaluates to a value of 1.0587 (Gemson, 1991). The $\mathbf{R}$ can be obtained from the variance of the magnetometer heading readings during a period of constant orientation. From the variance calculated in figure 6, $\mathbf{R}$ is determined to be 1.0585. Now the Kalman gain $\mathbf{K_k}$ is calculated.

$$\mathbf{K}_k = \mathbf{P}_{k|k-1}\mathbf{H}_k^{T}\left(\mathbf{H}_k\mathbf{P}_{k|k-1}\mathbf{H}_k^{T} + \mathbf{R}_k\right)^{-1} \tag{7}$$

Now the kalman gain k can be calculated using the observation matrix $H = 1$, since the magnetometer measurements will provide the heading angle with $\psi_c = 2\pi - \text{atan}\,(H_y/H_x)$. This Kalman gain will be used to correct the predicted state, with a larger value indicating a larger change to the state estimate and state covariance given the magnetometer measurements.

$$\hat{\mathbf{x}}_k = \hat{\mathbf{x}}_{k|k-1} + \mathbf{K}_k \left(\mathbf{z}_k - \mathbf{H}_k \hat{\mathbf{x}}_{k|k-1}\right) \tag{8}$$

$$\mathbf{P}_k = \left(\mathbf{I} - \mathbf{K}_k \mathbf{H}_k\right) \mathbf{P}_{k|k-1} \tag{9}$$

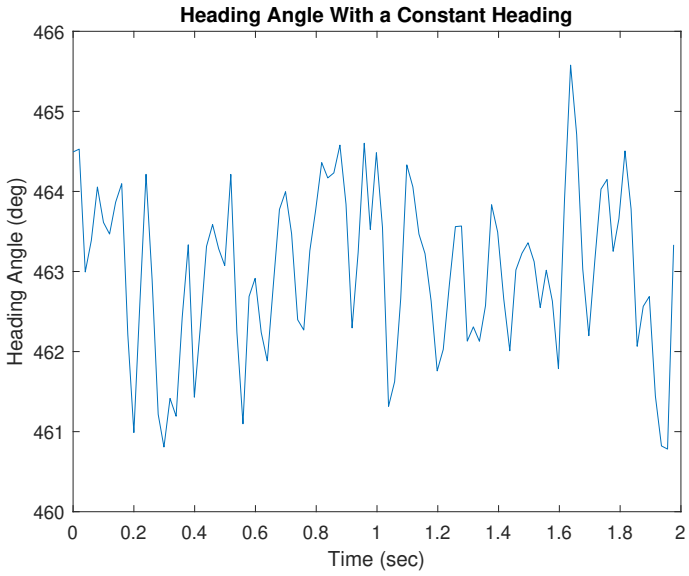

Figure 6: Magnetometer variance

5 Results

5.1 Walking

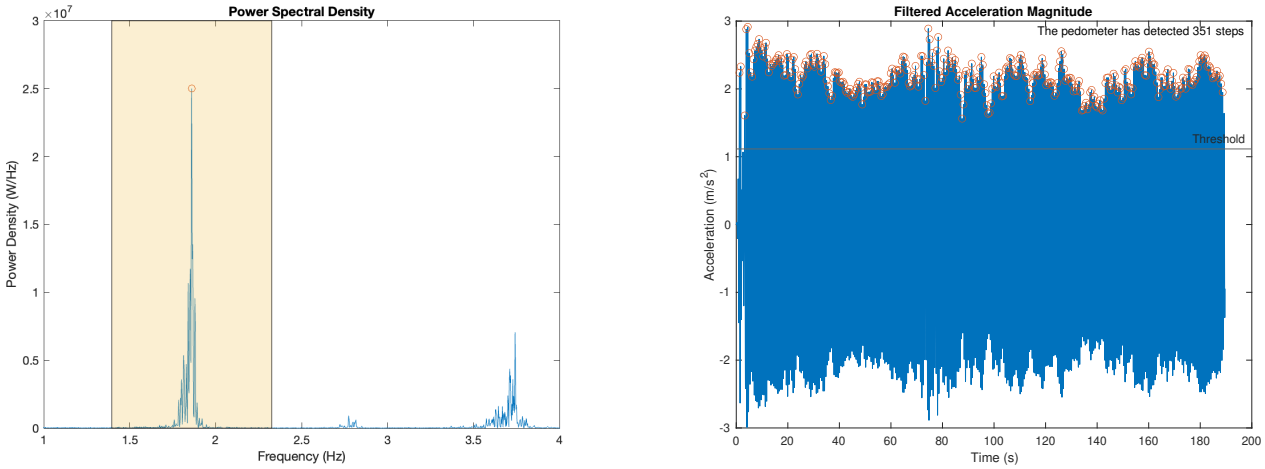

(a) Power Spectral Density for Walk

(b) Walking Steps Detected

Figure 7: Pedometer Data for Step Detection.

Using the pedometer data, the band-pass filter is chosen with the dominant walking frequency of around 1.75Hz as seen in Figure 11a. This detected 351 steps during the walk. Using the distance estimator described in Equation 1, the step length is calculated as 0.664m.

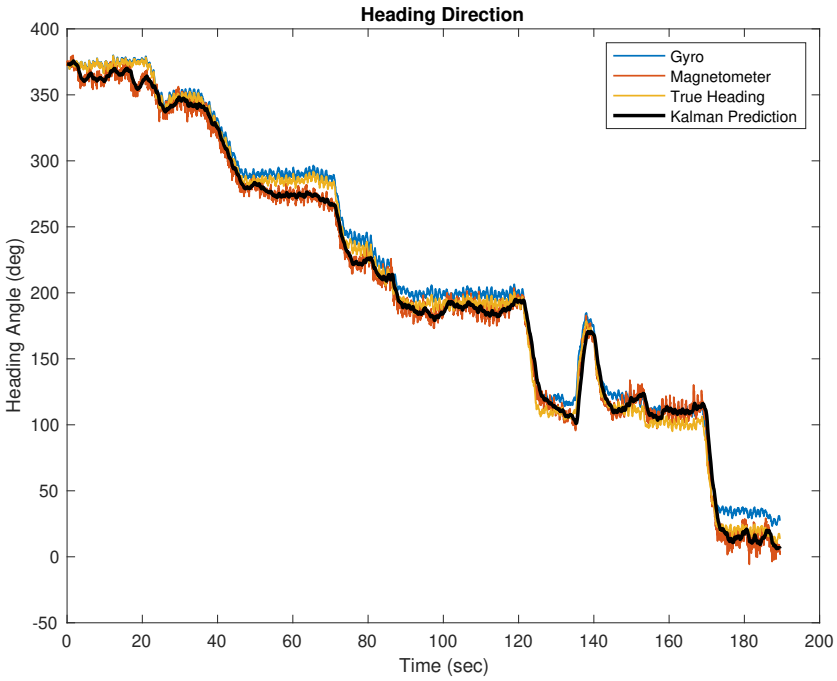

Figure 8: Heading Direction for Walk

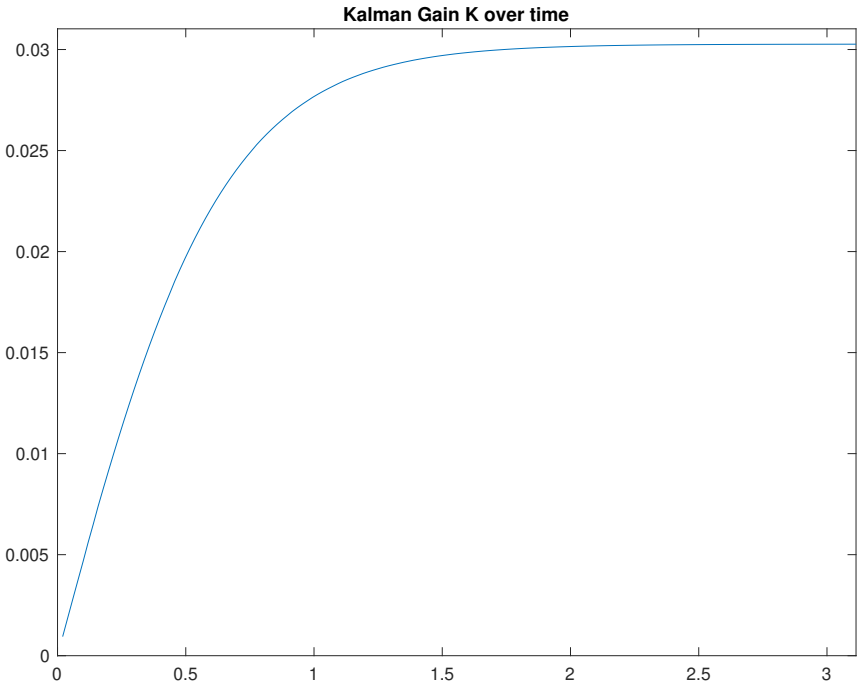

Figure 9: Kalman gain convergence

The heading direction estimates using the various sensors can be seen in Figure 8. Comparing the Kalman prediction to the true heading using the orientometer, the Kalman prediction follows the true orientation accurately. The predicted signal favours the magnetometer readings and smooths the fluctuations of its signal. Looking at the convergence of the Kalman Gain in Figure 9, the value of K converges in approximately 3 seconds to 0.03. This means that there is only a small correction to the predicted state estimate.

Figure 10: Walking Path Results

The results of using this Kalman heading prediction and step length produces the walking path as seen in Figure 8. To evaluate the results to the GPS data, we have to interpolate the recorded GPS data to match the sampling rate of the sensors, since the GPS module records data at a much lower frequency. After linear interpolation of the GPS data, the MSE is 59.12m.

5.2 Running path

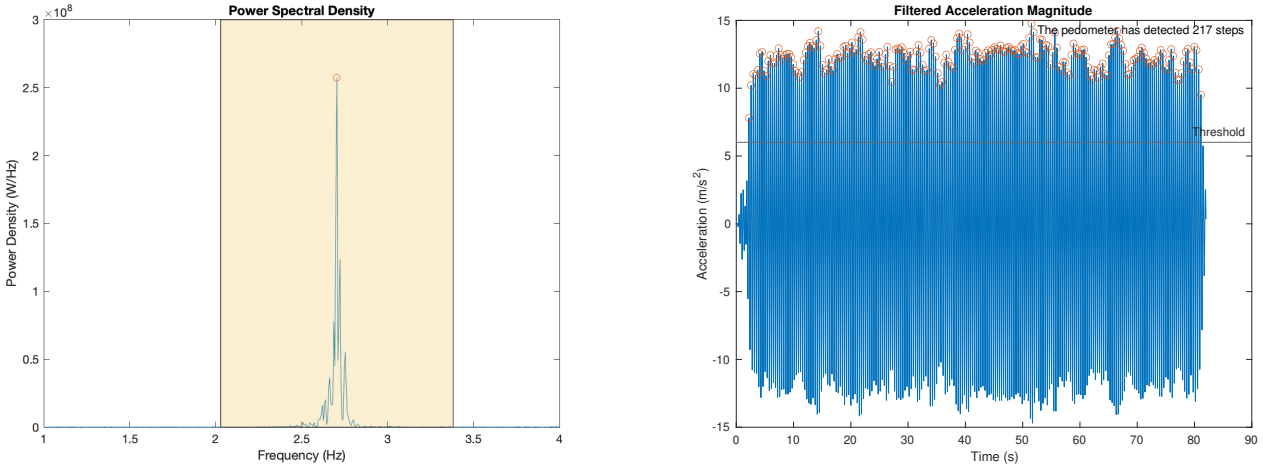

(a) Power Spectral Density for Run

(b) Walking Steps Detected

Figure 11: Pedometer Data for Step Detection.

The dominant frequency for the run is 2.7Hz. Using a bandpass filter around this range, the pedometer has detected 217 steps

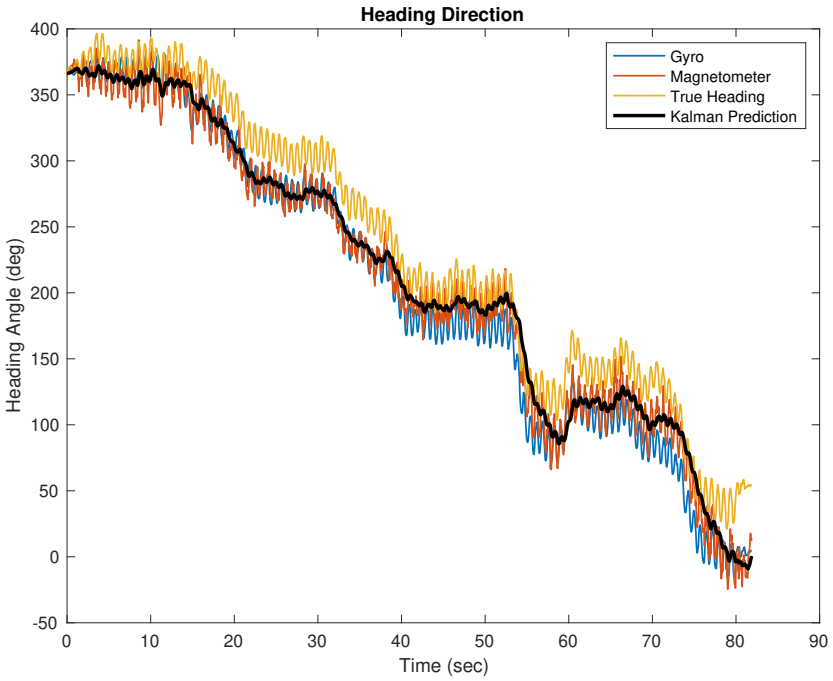

Figure 12: Heading Direction for Run

The Kalman prediction for the run follows the true orientation accurately as seen in Figure 12. There are greater oscillations for all the measurements recorded due to the larger bounce experienced between running steps.

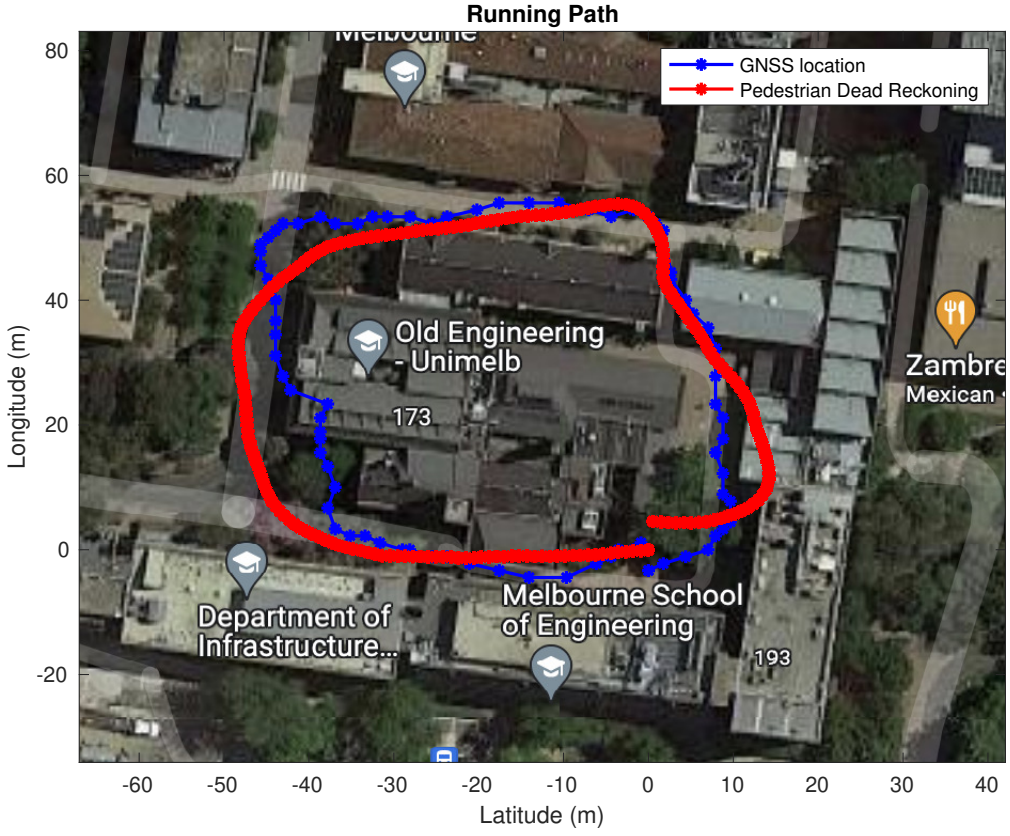

Figure 13: Running Path Results

The results for the running scenario leads to a MSE of 16.34m after linear interpolation of the GPS

data

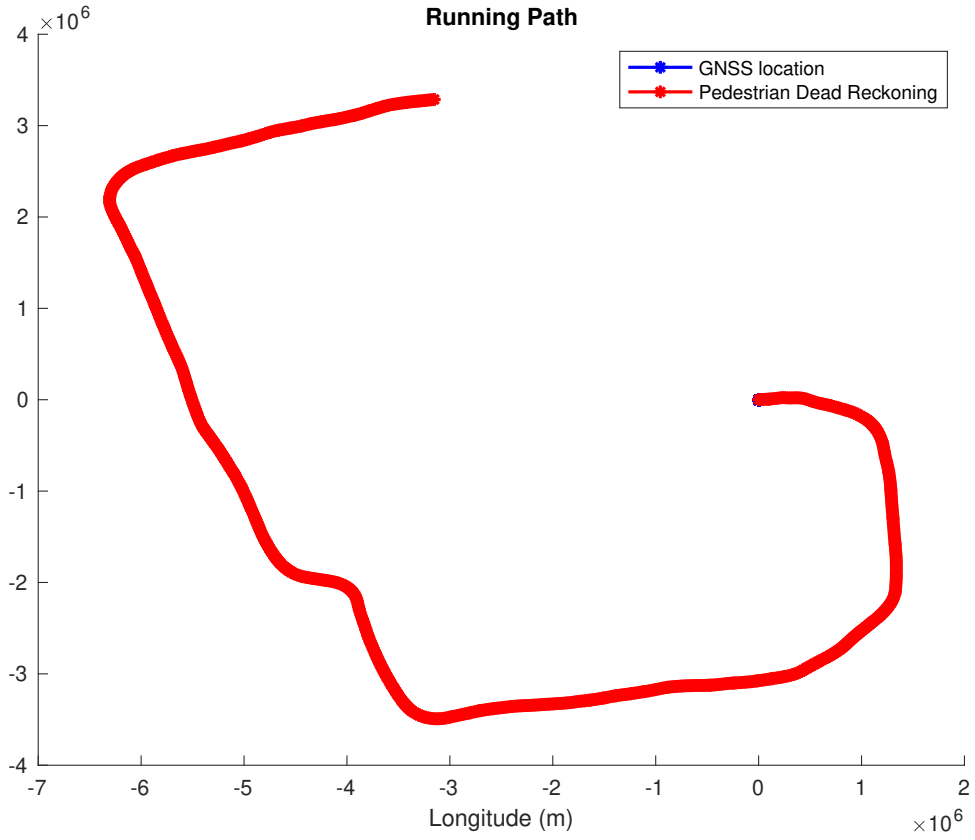

Figure 14: Running Path Results

This figure represents the walk using the integration method as the distance estimator, which produces a MSE of 6.98E+12m.

6 Discussion

Overall, utilising the adaptive step length algorithm in equation 1 that uses the z acceleration during the walk to predict the step length combined with the Kalman filter produced accurate results. The walk around the Old Engineering building led to a MSE of 59.12m, while the run around the same route led to a MSE of 16.34m.

The MSE of the run is lower than the walk, which could be due to the shorter time period of the run. This means that the the accumulation of drift error from integration of the angular velocity signal that has Gaussian white noise is reduced, leading to more accurate results.

However, this accuracy is only valid when the phone is held at a constant pitch of 0, which is not a realistic assumption as this pitch angle can fluctuate during the walk. In order to improve this, the 3-axis accelerometer can be used to predict the orientation of the phone during the walk, and the results of the gyro and magnetometer can be corrected based off the measured roll, pitch and yaw angles.

References

Gemson, R. (1991). Estimation of aircraft aerodynamic derivatives accounting for measurement and process noise by ekf through adaptive filter tuning. *Bangalore, India: Department of Aerospace Engineering, Indian Institute of Science*.

Kaniewski, P., & Kazubek, J. (2009). Integrated system for heading determination. *Acta Physica Polonica-Series A General Physics*, *116*(3), 325.

Ozyagcilar, T. (2012). Calibrating an ecompass in the presence of hard and soft-iron interference. *Freescale Semiconductor Ltd*, 1–17.

Rhudy, M. B., Salguero, R. A., & Holappa, K. (2017). A kalman filtering tutorial for undergraduate students. *International Journal of Computer Science & Engineering Survey*, *8*(1), 1–9.

Weinberg, H. (2002). Using the adxl202 in pedometer and personal navigation applications. *Analog Devices AN-602 application note*, *2*(2), 1–6.